Large-eddy simulation of lock-exchange gravity currents around a mounted rectangular cylinder

Zhihuan Hu[1,2], Xin Li[1,2], Jianmin Yang[1,2], Jun Li[1,2], Lei Wang[1,2]

[1]State Key Laboratory of Ocean Engineering, Shanghai Jiao Tong University,

Shanghai, 200240, China

[2]Collaborative Innovation Center for Advanced Ship and Deep-Sea Exploration,

Shanghai, 200240, China

Abstract

The dynamics of the lock-exchange gravity current around a mounted rectangular cylinder are investigated using three-dimensional large eddy simulations. The transient impact forces acting on the cylinder exerted by current, as well as flow fields around the cylinder are presented. Such a lock-exchange gravity current could make strong fluctuations of the lift and drag forces on the cylinder. With the validation and convergence studies, the numerical simulations in this paper could provide useful information for the unsteady flow fields of the gravity current and associated forces acting on the cylinder.

Introduction

Gravity currents occur infrequently and unpredictably in many natural environment and engineering applications. When such currents encounter the marine structures, considerable force acting on the structures could pose a challenge to the marine structures, such as submarine pipeline operation, submerged tunnel installation and cable laying of ROVs. For example, cable breaks occur in the Congo-Zaire submarine fan every 1 or 2 years due to particle-driven gravity currents [1]. Thus, the knowledge of dynamic load on submarine engineering structures can be of great value.

Significant efforts have been taken to investigate the gravity currents produced by lock exchange, where a heavier fluid propagates into a lighter one driven by the density difference between the fluids. Benjamin [2] developed a hydraulic theory which assumes conservation of mass and momentum, to describe the front speed and height of gravity current. He also suggested that the dynamics of gravity currents be strongly influenced by energy dissipation due to turbulence and mixing between the heavier fluid and ambient one. Although there is mixing, an alternative theoretical treatment by Shin et al. [3] showed that dissipation is not important at high Reynolds number. His theory based on energy-conserving flow could describe the front Froude number in lock-exchange experiments satisfactorily. Assuming that the pressure field is purely hydrostatic, Huppert [4] applied a shallow-water approach to evaluate the evolution of low-Reynolds-number gravity currents. This assumption may hold for small-particle gravity current.

More recent investigations have explored the interaction between a lock-exchange gravity current and a mounted obstacle. Lock-exchange experiments by Ermanyuk et al. [5] measure the drag and lift forces acting on a square cylinder generated by gravity current. Applying a similar lock-exchange configuration, Gonzalez-Juez et al. [6] presented the time-varying drag and lift coefficients over a mounted square cylinder by means of large-eddy simulations. Such drag and lift fluctuations showed a good agreement with previous experimental results. By replacing a single body with a periodic array of obstacles, Tokyay et al. [7]

showed these obstacles could increase the drag force acting on the current. The back-propagating hydraulic jump, along with the strong intensified mixing vortex are observed when the flow impinges on the bottom-mounted obstacles.

In this study, numerical investigations of gravity current impinging on a mounted rectangular cylinder are performed. We employ the generic case in the partial-depth, lock-exchange configuration based on the Boussineq approximation. The temporal evolution of the interaction between gravity current and mounted cylinder is divided into two qualitatively different phases: the slumping phase where the denser flow does not reach the cylinder; and the drag-important phase in which the denser flow reaches and then propagates over the cylinder. The transient drag and lift forces are presented and discussed in detail. Conclusions are drawn at the end of this study.

Numerical model and basic equations

System description

We consider the partial-depth gravity current, where the denser fluid of density ρ_2 and concentration c_2 occupies the depth $h < H$, as shown in Fig. 1. A channel of length L, height H and width w is filled with ambient fluid of density ρ_1 and concentration c_1. The flow is started by vertically removing the gate at $x = 0$, and current forms and propagates towards a mounted cylinder. Then it encounters a mounted cylinder at a distance l_c. The parameter values of the given system are listed in Table 1.
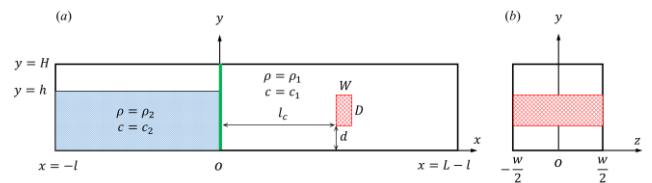

Figure. 1. Schematic of flow configuration: (a) side view and (b) streamwise view

Table 1 Main parameters in the 3-D numerical simulation

Parameter	Reference Case	Parameter	Reference Case
L/h	40	d/h	0.00625
l/h	20	W/h	0.125
H/h	1.25	D/h	0.25
w/h	1.25	Re	7049
l_c/h	7.125	Sc	10

Governing equations and numerical methods

The Navier-Stokes equations are usually made dimensionless using the flow depth h and the buoyancy velocity u_b [8]

$$u_b = \sqrt{g^* h}$$
$$g^* = g(1 - \gamma)$$

$$\gamma = \frac{\rho_1}{\rho_2}$$

The density differences are relatively small and thus we assume the linear relationship between density and concentration.

$$\rho = \rho_1 + \frac{\rho_2 - \rho_1}{c_2 - c_1}(c - c_1)$$

The dimensionless variables can be defined as

$$t^* = \frac{t}{h/u_b}, x_i^* = \frac{x_i}{h}, u_i^* = \frac{u_i}{u_b}, p^* = \frac{p}{\rho_1 u_b^2}, c^* = \frac{c - c_1}{c_2 - c_1}$$

Where p^*, u_i^* and c^* denote the total pressure, velocity vector and concentration, respectively. Then, we obtain the basic equations based on the conversation of mass, momentum and concentration in the dimensionless form.

$$\frac{\partial u_j^*}{\partial x_j^*} = 0,$$

$$\frac{\partial u_i^*}{\partial t^*} + \frac{\partial (u_i^* u_j^*)}{\partial x_j^*} = -\frac{\partial p^*}{\partial x_j^*} + \frac{\partial}{\partial x_j^*}\left(\left(\frac{1}{Re} + v_{sgs}^*\right)\left(\frac{\partial u_i^*}{\partial x_j^*} + \frac{\partial u_j^*}{\partial x_i^*}\right)\right) + c^* e_i^g$$

$$\frac{\partial c^*}{\partial t^*} + \frac{\partial (c^* u_j^*)}{\partial x_j^*} = \frac{\partial}{\partial x_j^*}\left(\left(\frac{1}{Re \cdot Sc} + \kappa_{sgs}^*\right)\frac{\partial c^*}{\partial x_j^*}\right)$$

Where e_i^g indicates the unit vector in the direction of gravity. The Reynolds and Schmidt numbers are thus identified in the governing equations

$$Re = \frac{u_b h}{v}, Sc = \frac{v}{\kappa}$$

Where v represents the kinematic viscosity and κ the molecular diffusivity. For large-eddy simulations (LES), the above equations contain subgrid-scale stress (SGS) terms, namely, the SGS viscosity v_{sgs}^* and diffusivity κ_{sgs}^*. One-equation eddy-viscosity model is used to evaluate v_{sgs}^* and κ_{sgs}^* [9]. The N-S equations are discretized using the finite volume method (FVM) in OpenFOAM.

Convergence and validation studies

Bottom-mounted cylinders with a gap of $0.00625h$ between the bottom wall and the cylinder bottom is considered to reproduce the experimental conditions [5]. The non-slip boundary condition is employed along the bottom ($y = 0$), left ($x = -l$), right ($x = L - l$), front ($z = w/2$) and rear ($z = -w/2$) boundaries. The top boundary ($y = H$) is treated as a slip wall. The lock gate is located at $x = 0$, and fluid is initially at rest with $c^* = 1$ for denser fluid and $c^* = 0$ for ambient one. The time step was equal to $0.001h/u_b$ to keep the Courant-Friedrich-Lewy (CFL) number below a suitable value.

Front velocity

After a short initial acceleration produced by lock exchange, gravity currents reach the slumping phase where the front velocity V is close to constant. Given the Froude number based on the lock depth h

$$F_h = \frac{V}{\sqrt{g^* h}}$$

Shin et al. [3] obtained the dimensionless front velocity based on the energy-conserving theory, which assumes that there are no energy fluxes in and out of its boundaries.

$$F_h^2 = \frac{2 - \frac{h}{H}}{2\left(2 + (1 - \gamma)\frac{h}{H}\right)} \approx \frac{1}{2} - \frac{h}{4H}$$

and shallow-water theory

$$F_h^2 \approx 0.45125 - 0.20125\frac{h}{H}$$

It does not make the energy-conserving assumptions, for waves can be generated along the interface between the denser and lighter fluid. Therefore, the front velocity predicted by shallow-water theory could be slightly smaller than the energy-conserving theory.

In order to validate the numerical model, as well as evaluate the effects of grid on the simulation results, comparisons of F_h between three different grid resolutions are performed, as listed

in Table 2. The numerical results are observed to be slightly smaller than theoretical valus. Such little discrepancy is thought to be a consideration of energy dissipation due to the turbulent mixing in the simulations. The Kelvin-Helmholtz (KH) instability, along with the KH vortices are observed across the interface between two fluids, due to the sharp difference of velocity in the interfacial fluid. And the unsteady flow could easily develop into turbulence, thereby intensifying the mixing of two fluids.

Table 2 Main parameters in the 3-D numerical simulation

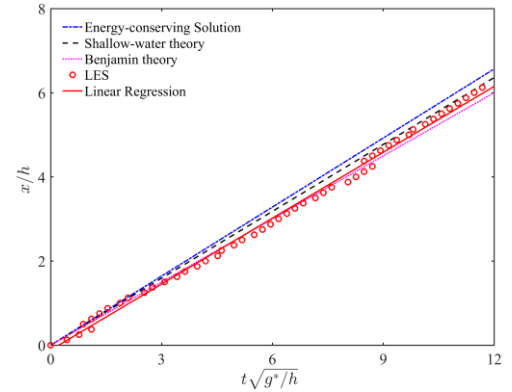| Case	Mesh	Elements	F_h
Case1	fine	4,142,000	0.527
Case2	medium	2,136,500	0.522
Case3	coarse	1,438,400	0.524
Energy-conserving theory			0.547
Shallow-water theory			0.539

Figure. 2. Comparison of time-varying front position (x/h) of gravity current at slumping phase. Linear regression of numerical results is plotted in red solid line.

Drag and lift coefficients

The spanwise-averaged drag and lift coefficients of the rectangular cylinder are defined as

$$C_D = \frac{2F_x}{\rho_1 w D V^2}$$

$$C_L = \frac{2F_y}{\rho_1 w D V^2}$$

Where F_x and F_y are the streamwise and transverse force acting on the cylinder, respectively. The comparisons of time-varying C_D and C_L are shown in Fig. 3, which demonstrates good overall agreement. A noticeable difference concerns the first impact of gravity currents on the mounted cylinder. And it could be caused by the low data-sampling rate of the experiments, thereby underestimating the first peak of impact loads.
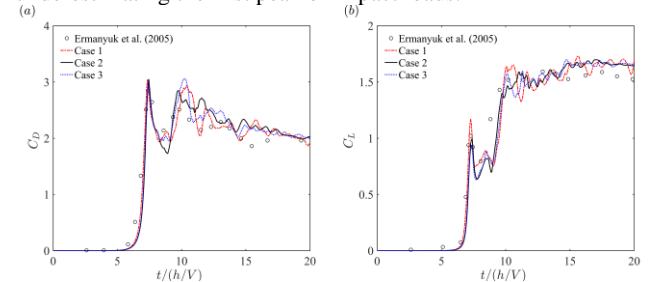

Figure. 3. Comparisons of temporal evolution of the drag (a) and lift (b) coefficients.

It is concluded that the numerical model in the present study shows a good agreement with the experimental results, as well as a good convergence for the spatial resolutions. In order to simulate the flow with a better accuracy, the fine mesh with 2136500 elements are adopted for the lock-exchange gravity current.

Results and discussion

In this section, numerical results of the interaction between the gravity current and mounted cylinder at three different depths are presented.

Results for bottom-mounted cylinder ($d/h = 0.00625$)

Lift and drag coefficients

The force F_i acting on the cylinder by the fluid is obtained as

$$F_i = P_i + V_i$$

$$P_i = \int_A -n_i p \ \mathrm{d}A$$

$$V_i = \int_A n_j \mu \left(\frac{\partial u_i}{\partial x_j} + \frac{\partial u_j}{\partial x_i} \right) \mathrm{d}A$$

Where A indicates the surface of cylinder, n_j its outer normal. We eliminate the initial hydrostatic pressure when evaluating the lift force. The x and y components of F_i are defined as drag F_D and lift F_L, respectively.

Fig. 4 shows the time variations of dimensionless lift and drag forces. A sharp increase in the lift and drag forces acting on the cylinder can be observed at the drag-important phase. Then they peak at approximately $\bar{t} = 7.446$. It is clear that the viscous lift and drag components are much smaller than the pressure components. This means that the pressure forces dominate the impact forces exerted by fluid on the given cylinder.
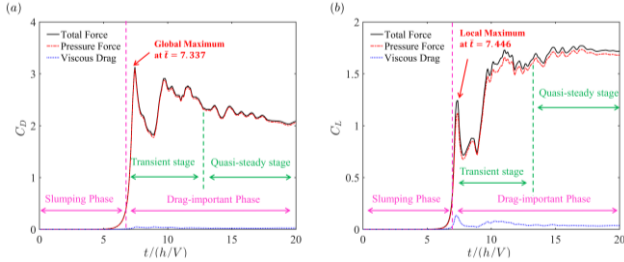

Figure. 4. Detailed variation of lift and drag coefficients with time for case 2, including the pressure forces and viscous components.

Structure of gravity current

To further understand such unsteady lift and drag generated by the interaction of gravity currents with the cylinder, the evolution and structures of flow field around the cylinder are discussed in detail.

As the denser fluid hits the upstream face of cylinder, its head of the high-velocity jet-like flow is deflected upward, thereby causing the splash of the mixed fluid, as shown in Fig. 5 (a). As the approaching gravity current decelerates, the pressure on the upstream face rises to a relatively high positive value (see Fig. 5 (b)) and thus generates the first drag maximum. Also the flow separation occurs at the sharp corner of the cylinder, as illustrated in Fig. 5 (c), which could also result in the increased drag. The mixed fluid flow past the cylinder creates the low-pressure vortices (see Fig. 5 (c)), which generates a negative-pressure region on the top of cylinder. The first lift maximum happens simultaneously, as a result of the relatively high negative pressure.

As the gravity current passed over the cylinder, it reattaches along the bed and eventually reaches a quasi-steady state. It can be seen from Fig. 4 that the lift and drag slowly vary with time. When the denser fluid continues to propagate downstream of the cylinder, the hydraulic jump occurs where the high-velocity flow discharges into a zone of lower velocity, as shown in Fig. 6 (a). The rapidly flowing denser liquid is abruptly slowed and increases in height, converting some of the kinetic energy into potential energy, with some energy dissipation accompanied by the intense turbulent mixing, entrainment and strong vortices. However, the flow does not become supercritical for the flow velocity is lower than the speed ($\sqrt{gh}$) of a shallow gravity wave. Similar phenomena could be found in the numerical simulations

by Gonzalez-Juez et al. [6]. Moreover, Fig. 6 (b) shows that the relatively large lift forces could be induced by the increase in pressure difference between the top and bottom face of the cylinder.
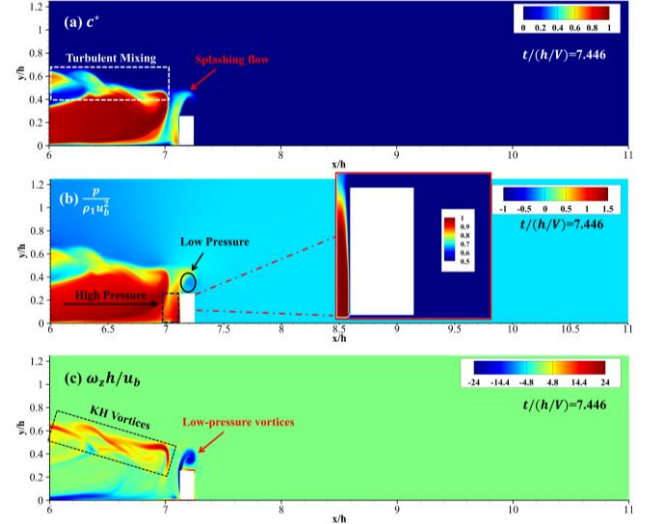

Figure. 5. Instantaneous flow fields for case 2 in $z = 0$ plane. (a) concentration; (b) pressure; (c) out-of-plane vorticity. The dimensionless time $\bar{t} = 7.446$
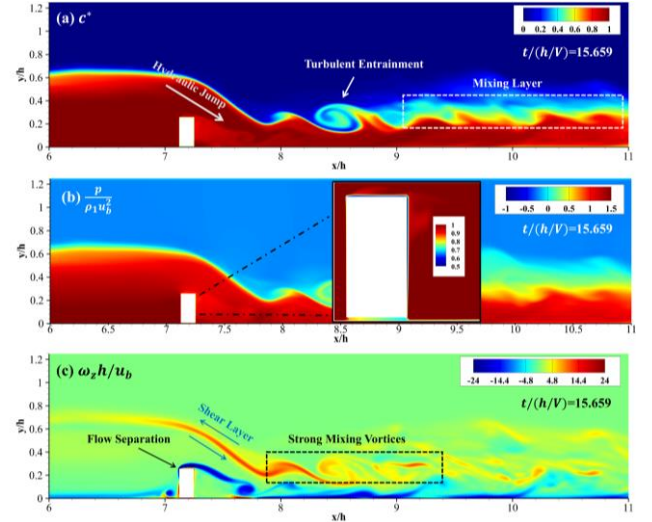

Figure. 6. Instantaneous flow fields for case 2 in $z = 0$ plane. (a) concentration; (b) pressure; (c) out-of-plane vorticity. The dimensionless time $\bar{t} = 15.659$

Results for $d/h = 0.25$

Lift and drag coefficients

For $d/h = 0.25$, the cylinder experiences a negative drag before the denser fluid impinges on it, and then the drag increases abruptly with the interaction of gravity current with the mounted cylinder. The large fluctuation of lift coefficient can also be observed in Fig. 7, from -0.71 to 0.53. Moreover, the extreme values of drag are always accompanied by the maximum or minimum value of lift.

Structure of gravity current

Fig. 8 provides the detailed information on the flow structures before the gravity current reaches the cylinder. The typical structure of the head, associated with the KH vortices at the interface of mixed flow that separates the denser fluid from the lighter one. As the gravity current approaches the cylinder, it accelerates the fluid in its vicinity, as shown in Fig. 8 (b). Thus a low-pressure region on the upstream face of the cylinder is generated, which lead to the negative drag on the cylinder.

Moreover, the approaching denser fluid increases the pressure on the bottom of the cylinder and therefore the particles in high-pressure region flow towards lower pressure. The velocity parallel to the cylinder boundary may be large, where the non-slip condition is maintained. Vorticity is created when such near-wall velocity gradients arise, thereby leading to the formation of a separated flow region (see Fig. 8 (c)).
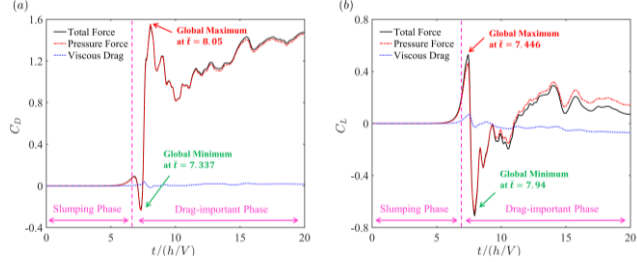

Figure. 7. Detailed variation of lift and drag coefficients with time for $d/h = 0.25$, including the pressure forces and viscous components.
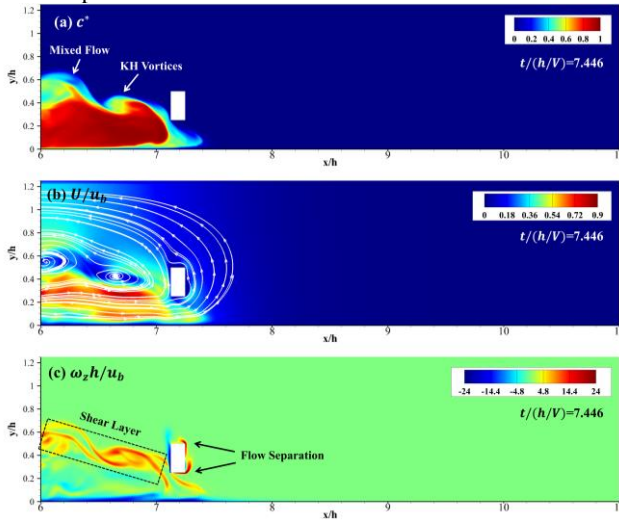

Figure. 8. Instantaneous flow fields for $d/h = 0.25$ in $z/h = 0.25$ plane. (a) concentration; (b) planar velocity $U = \sqrt{u_x^2 + u_y^2}$; (c) out-of-plane vorticity. The dimensionless time $\bar{t} = 7.446$

At $\bar{t} = 8.103$, when the front impacts the upstream face of the cylinder, the mainstream propagates over the bed with a higher speed. The height of the accelerating gravity current (dashed green line) reduces to a half of initial height (solid green line), as shown in Fig. 9 (a). A small proportion of the denser fluid moves upward due to the sudden change in the flow direction. The maximum height reached by the splashed fluid is slightly larger than the height of the cylinder. The fluid inside the splash starts to plunge downwards, with most of its momentum lost, at a low angle with the vertical, as illustrated in Fig. 9 (b). Thus a high-pressure region on the top of the cylinder is generated, along with a lower-pressure eddy on its bottom, thereby leading to a negative lift of large magnitude. Such a low-pressure eddy that are shed on the downstream and bottom face of the cylinder could be induced by the flow separation. Meanwhile, the density difference between the upstream and downstream face of the cylinder could introduce a large drag.

Conclusion

Three-dimensional simulations for $Re = 7049$ are applied to investigate the dynamic responses at two heights of the cylinder ($d/h = 0.00625$ and 0.25). Key conclusions are given below:

1. For the bottom mounted cylinder ($d/h = 0.00625$), the positive lift and drag coefficients undergo strong fluctuations and eventually reach a quasi-steady value. While for $d/h = 0.25$, the cylinder experiences the negative lift and drag of large magnitude, as well as smaller fluctuations.
2. The extreme values of drag force acting on the cylinder are associated with that of lift, when the gravity current impinges on the mounted cylinder.
3. The Kelvin-Helmholtz instability and the transient interaction between the gravity current and cylinder could intensify the turbulent mixing, thereby leading to stronger energy dissipation.
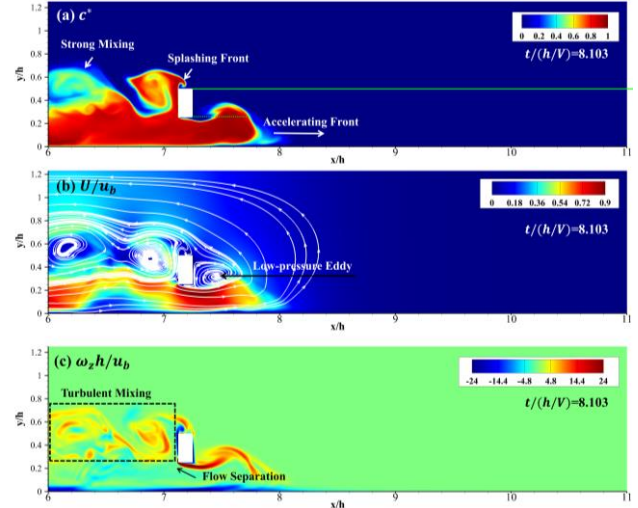

Figure. 9. Instantaneous flow fields for $d/h = 0.25$ in $z/h = 0.25$ plane. (a) concentration; (b) planar velocity $U = \sqrt{u_x^2 + u_y^2}$; (c) out-of-plane vorticity. The dimensionless time $\bar{t} = 8.103$

References

[1] Meiburg E, Kneller B. Turbidity currents and their deposits. Annual Review of Fluid Mechanics. 2010;42:135-56.
[2] Benjamin TB. Gravity currents and related phenomena. J Fluid Mech. 1968;31:209-48.
[3] Shin J, Dalziel S, Linden P. Gravity currents produced by lock exchange. J Fluid Mech. 2004;521:1-34.
[4] Huppert HE. Gravity currents: a personal perspective. J Fluid Mech. 2006;554:299-322.
[5] Ermanyuk EV, Gavrilov NV. Interaction of Internal Gravity Current with an Obstacle on the Channel Bottom. Journal of Applied Mechanics and Technical Physics. 2005;46:489-95.
[6] Gonzalez-Juez E, Meiburg E, Constantinescu G. Gravity currents impinging on bottom-mounted square cylinders: flow fields and associated forces. J Fluid Mech. 2009;631:65-102.
[7] Tokyay T, Constantinescu G, Meiburg E. Lock-exchange gravity currents with a high volume of release propagating over a periodic array of obstacles. J Fluid Mech. 2011;672:570-605.
[8] Tokyay T, Constantinescu G, Gonzalez-Juez E, Meiburg E. Gravity currents propagating over periodic arrays of blunt obstacles: Effect of the obstacle size. Journal of Fluids and Structures. 2011;27:798-806.
[9] Nakayama A, Vengadesan S. On the influence of numerical schemes and subgrid–stress models on large eddy simulation of turbulent flow past a square cylinder. International journal for numerical methods in fluids. 2002;38:227-53.